NASA CONTRACTOR REPORT 165636

AN INVESTIGATION FOR THE DEVELOPMENT OF AN INTEGRATED OPTICAL DATA PREPROCESSOR

C. M. VERBER, R. P. KENAN, N. F. HARTMAN
AND C. M. CHAPMAN

BATTELLE MEMORIAL INSTITUTE
COLUMBUS, OH 43201

CONTRACT NAS1-14655
OCTOBER 1980

National Aeronautics and
Space Administration

Langley Research Center
Hampton Virginia 23665

NASA CONTRACTOR REPORT 165636

AN INVESTIGATION FOR THE DEVELOPMENT OF AN INTEGRATED OPTICAL DATA PREPROCESSOR

C. M. VERBER, R. P. KENAN, N. F. HARTMAN
AND C. M. CHAPMAN

BATTELLE MEMORIAL INSTITUTE
COLUMBUS, OH 43201

CONTRACT NAS1-14655
OCTOBER 1980

National Aeronautics and
Space Administration

Langley Research Center
Hampton, Virginia 23665

TABLE OF CONTENTS

TABLE OF CONTENTS
(Continued)

LIST OF FIGURES

LIST OF FIGURES
(Continued)

SUMMARY

This report discusses the results of a program which culminated in the successful fabrication and the preliminary testing of a laboratory model of a 16-channel integrated-optical data preprocessor. The preprocessor was conceived in response to a need for a device to evaluate the outputs of a set of remote sensors. It does this by accepting the outputs of these sensors, in parallel, as the components of a multidimensional vector descriptive of the data, and comparing this vector to one or more reference vectors which are used to classify the data set. The comparison is performed by taking the difference between the signal and reference vectors.

The preprocessor is wholly integrated upon the surface of a $LiNbO_3$ single crystal with the exceptions of the source, and the detector. He-Ne laser light is coupled in and out of the waveguide by prism couplers. The integrated optical circuit consists of a titanium-infused waveguide pattern, electrode structures and grating beam-splitters. The waveguide and electrode patterns, by virtue of their complexity,make the vector-subtraction device the most complex integrated optical structure fabricated to date. The fact that this device has performed successfully in its preliminary tests is indicative of the progress being made in integrated-optics technology.

I. INTRODUCTION

This report summarizes a program which resulted in the successful fabrication of an integrated optical circuit (IOC) which, by interferometric means, is capable of determining the magnitude of the difference of two 16-dimensional vectors. The original concept for this device was generated during a NASA-sponsored program entitled "Feasibility Investigation of Integrated Optics Fourier Transform Devices (NASA-CR-2869, 1977) and was further refined during a subsequent program on "An Investigation for the Development of an Integrated Optical Data Preprocessor" (NASA-CR-3151, 1979).

The 16-channel vector subtraction IOC is, by virute of its overall size, complex waveguide pattern and intricate electrode structure, the most complex IOC yet fabricated in any laboratory. The principle goal of this program was to show that such a complex device could, indeed, be fabricated and within limits, operate as predicted. We have accomplished the first of the goals and, according to the minimal testing carried out to date, appear to have accomplished the second. In the process of achieving these goals the following have been accomplished.

- Fabrication of a complex horn structure for disecting and subsequently reassembling a multimode guided wave with only minimal wavefront perturbation.
- Perfection of photolithographic alignment techniques accurate to better than 10^{-4} radian.
- Development of high quality As_2S_3 overlay gratings for beam splitters and combiners.
- Development of a mathematical description of the operation of the preprocessor.

In this report we briefly review the intended role of the processor and some of the preceding work in a Background Section. We then discuss the Principles of Operation, Design and Component Studies, and Fabrication of the device and finally present some preliminary Test Results. We may conclude from this program that it is feasible to fabricate relatively complex IOC's and that the present device could form the basis for an operational vector-subtraction preprocessor.

II. BACKGROUND

ROLE OF THE PREPROCESSOR

The various NASA missions which are dedicated to the remote sensing of terrestrial features are characterized by the acquisition, transmission, storage and processing of enormous amounts of data. As is suggested in Figure II-1, a large fraction of this data is, for one reason or another considered useless and is therefore discarded. A major failing of present data handling systems is that processing this useless data accounts for a substantial part of the total time lag between data acquisition and delivery of the data to the customer in a usable form. This program deals with the design and construction of an integrated optical data preprocessor which is designed to alleviate this situation in cases where the data are in the form of sets of analog voltages delivered simultaneously from a number of sensors. In its simplest form, the function of the preprocessor is to provide a signal indicating whether an incoming data set is useful or useless according to some predetermined criteria (Fig. II-2). A more advanced version of the preprocessor should be capable of performing a classification or identification function (Fig. II-3), thereby affecting even greater economies in the transmission, storage and processing of the data acquired by remote sensors.

The basic operation which the preprocessor is designed to perform is the generation of an output signal which is proportional to the sum of the absolute values of a function of the channel by channel difference of the signal and reference voltages. As will be discussed in detail below, this operation is accomplished by optical interferometry after first utilizing the electrooptic effect to generate an optical phase analog of the N simultaneous voltages which comprise the input data set. The simplest application of this operation is in the screening mode which is indicated schematically in Figure II-4. As an example of its utility, consider the case of a multispectral scanner whose mission is to look for perturbations in the spectral signature of the sunlight reflected from the ocean due to oil spills, plankton, etc. If the preprocessor is programmed with the reference set characteristic of clear sea water, then it will generate a signal greater than some predetermined threshold value only when the incoming data indicate a

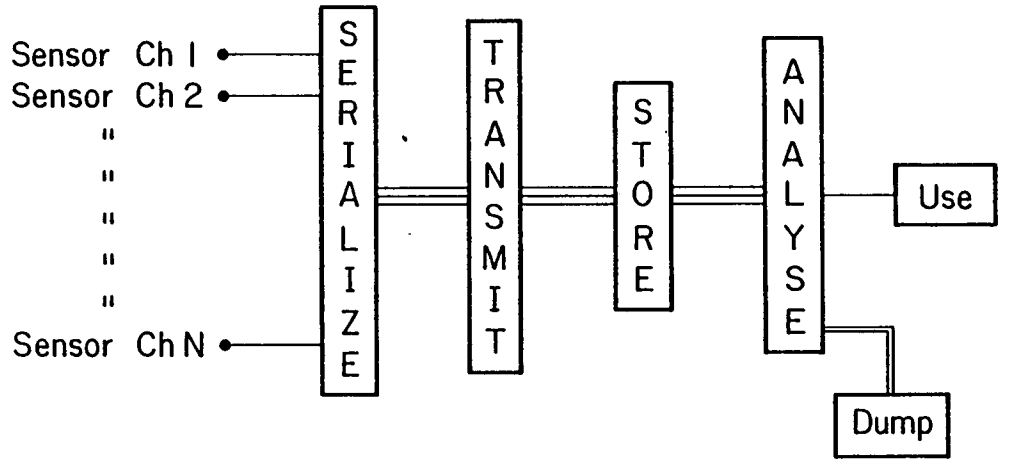

FIGURE II-1. CURRENT PROCEDURE FOR HANDLING REMOTELY ACQUIRED, MULTI-SENSOR DATA. UNDESIRED DATA REPRESENT A SIGNIFICANT FRACTION OF THE SYSTEM LOAD.

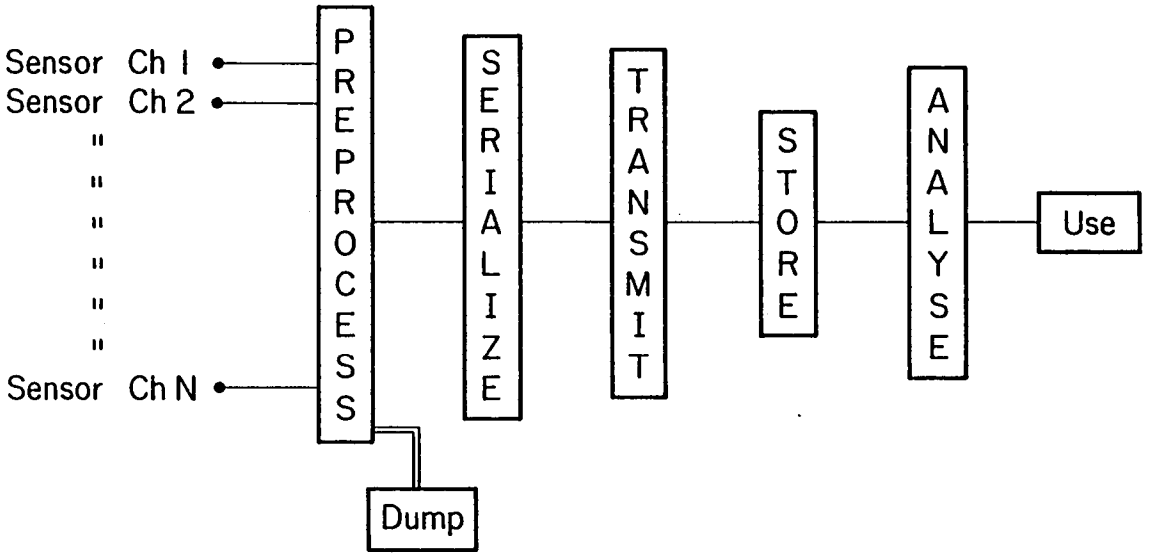

FIGURE II-2. USE OF A PREPROCESSOR TO ELIMINATE USELESS DATA PRIOR TO TRANSMISSION.

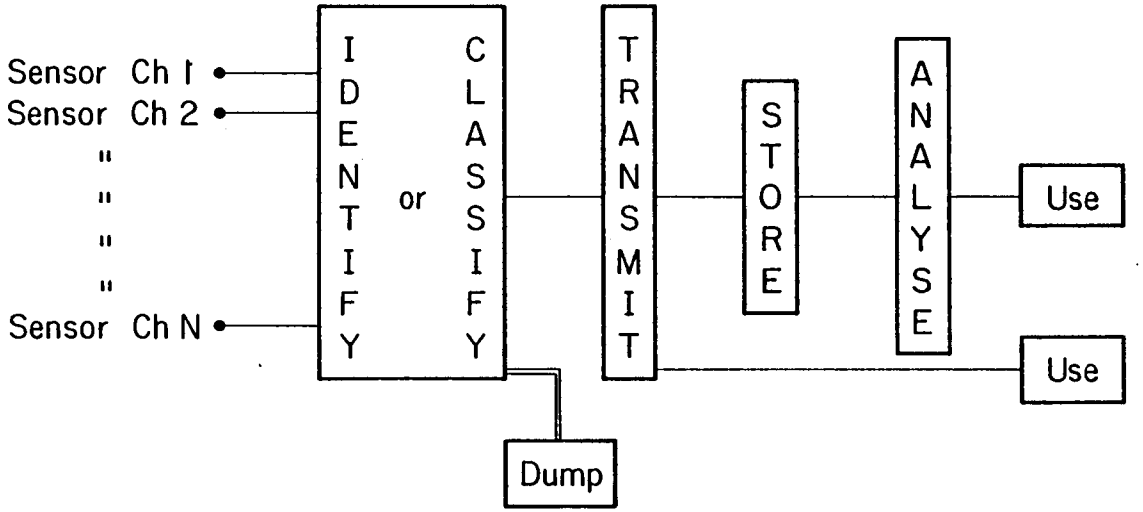

FIGURE II-3. USE OF A MORE ADVANCED PREPROCESSOR TO CLASSIFY DATA BEFORE TRANSMISSION.

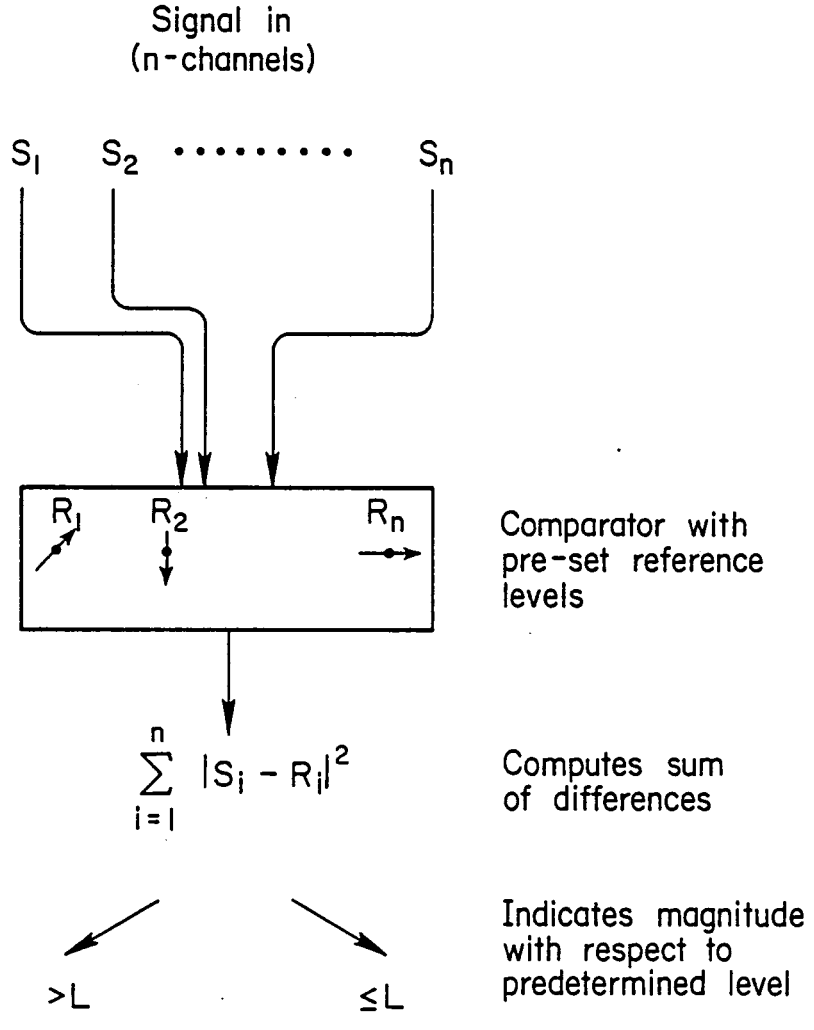

FIGURE II-4. SCHEMATIC REPRESENTATION OF A PREPROCESSOR OPERATING IN A SCREENING MODE.

significant departure from the clear water spectrum. All unflagged data will be dumped before transmission, effecting an estimated 95% reduction in data load.

A more sophisticated mode of operation of the preprocessor is the classification or identification mode (Fig. II-5). Here, the data set to be identified is compared to a large number of reference sets which can be read into the preprocessor from some parallel storage medium, e.g., an N-track magnetic tape. The identification occurs when the comparison of the data to a particular reference set results in a null output from the preprocessor. Obviously this mode of operation will be useful when it is anticipated that the incoming data will represent one of a finite number of previously characterized situations.

Previous Work

In an earlier phase of this work, a three-channel preliminary version of the preprocessor was fabricated and tested.[1] This device, which is shown in Fig. II-6, was fabricated on an outdiffused $LiNbO_3$ waveguide and utilized a waveguide hologram to perform the required interferometric subtraction. Its successful operation demonstrated the soundness of the optical approach and the ability to integrate a number of components upon a single substrate to form an integrated optical circuit (IOC). On the basis of this success, it was decided to construct a 16-channel preprocessor which would have the potential for being tested with simulated and actual sets of multispectral data.

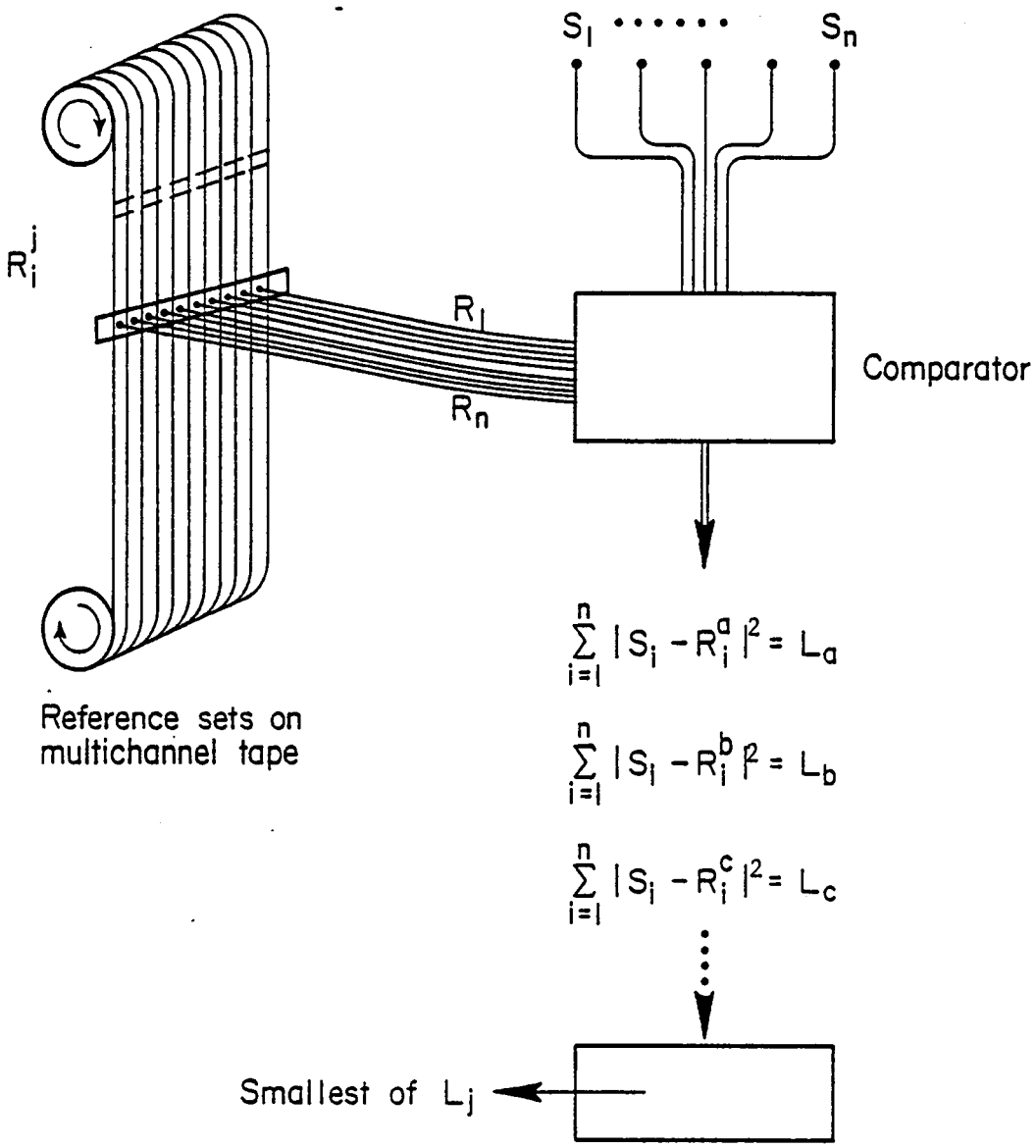

FIGURE II-5. SCHEMATIC REPRESENTATION OF A PREPROCESSOR OPERATING IN AN IDENTIFICATION MODE.

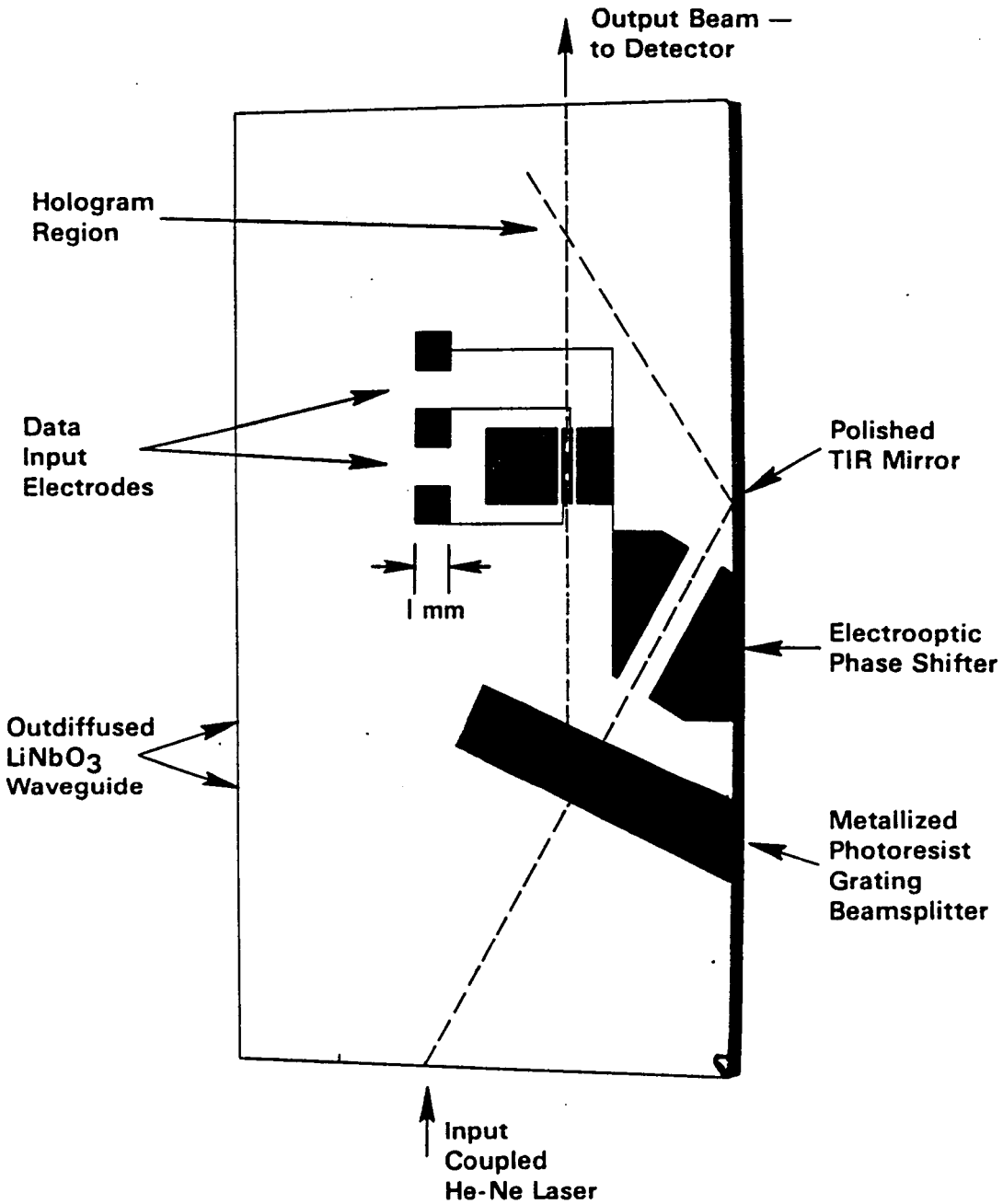

FIGURE II-6. PHOTOGRAPH OF THREE-CHANNEL LABORATORY MODEL SHOWING ELECTRODE STRUCTURES.

III. PRINCIPLES OF OPERATION

FEATURE IDENTIFICATION BY VECTOR SUBTRACTION

The output of a multispectral sensor system is a set of signal voltages $\{V_{Si}\}$, each voltage being proportional to the reflected light intensity in a given spectral band. The set $\{V_{Si}\}$ can be thought of as the components of a vector $\vec{V}_S$ in a multidimensional spectral space. If we have a set of reference data, $\{V_{Ri}\}$, the members of which are the components of a reference vector $\vec{V}_R$ in the same space, then we can define the difference between the two sets as the scalar distance d between them in the N-dimensional spectral space. This distance has the usual definition

$$d_{SR}^2 = \sum_{i=1}^{N} (V_{Si} - V_{Ri})^2 \qquad \text{(III-1)}$$

If $d_{SR} = 0$, then it is evident that $\{V_S\} \equiv \{V_R\}$, so an identification between the signal and reference sets has been established.

In the screening or data-editor mode of operation a threshold level L is chosen and all data for which $d_{SR}^2 < L$ is discarded. In this case, $\{V_R\}$ could represent the spectral signature of clear water, clouds, or any other feature which would be indicative of uninteresting data.

In the identification mode, there would be an entire set of reference vectors $\vec{V}_{Rj}$, j =1.....M each representing the signature of a given feature. In this case, determination of the minimum $(d_{SR}^2)_j$ would indicate which reference set most closely coincided with the signal set.

THE OPTICAL APPROACH TO VECTOR SUBTRACTION

The Mach-Zehnder Interferometer

The way in which the operation defined in Eq. (III-1) as well as other potentially useful mathematical operations can be performed by a multichannel interferometer can best be explained by looking first at the operation of the simple Mach-Zehnder interferometer with electrooptic phase shifters in

each arm as shown in Figure III-1. We will refer to Arm 1 and Arm 2 as the optical signal arm and the optical reference arm respectively. The light intensity seen at the detector is

$$I = \left|Se^{is} + Re^{ir + \Delta}\right|^2 = S^2R^2 + 2SR \cos (s-r-\Delta) \qquad \text{(III -2)}$$

where S and R are the amplitudes of the two beams at the detector and s and r+Δ are their respective relative phases. In terms of Figure 1, s is proportional to $(V_R - R_S)$ and Δ is proportional to V_Δ. The reason for introducing the additional phase r in the optical reference arm will be made clear below.

The Modified Mach-Zehnder Interferometer

Consider now the case in which the interferometer of Figure III-1 is modified so that the beam in both the signal arm (arm 1) and the reference arm (arm 2) are transversely divided into N equal segments each of which can be independently controlled. The intensity at the detector is now given by

$$I = \sum_{i=1}^{N_i} S_i^2 + R_i^2 + 2S_iR_i \cos (s_i - r_i - \Delta) \qquad \text{(III-3)}$$

Two assumptions are implicit in going from Eq. III-2 to Eq. III-3. First, it is assumed that there is no cross-talk between the channels. Second, diffraction effects are ignored. The latter assumption is one of convenience since the computational difficulties would be enormous if diffraction were included. It is justified by the fact that it is possible to design the device so that the beam combiner is in the near-field region in which diffraction effects have not yet fully developed. This limit Z of this region is given by

$$Z = \pi w^2/\lambda \qquad \text{(III-4)}$$

where Z is measured from the end of the confinement region, W is the width of the apparatus and λ the wavelength of light.

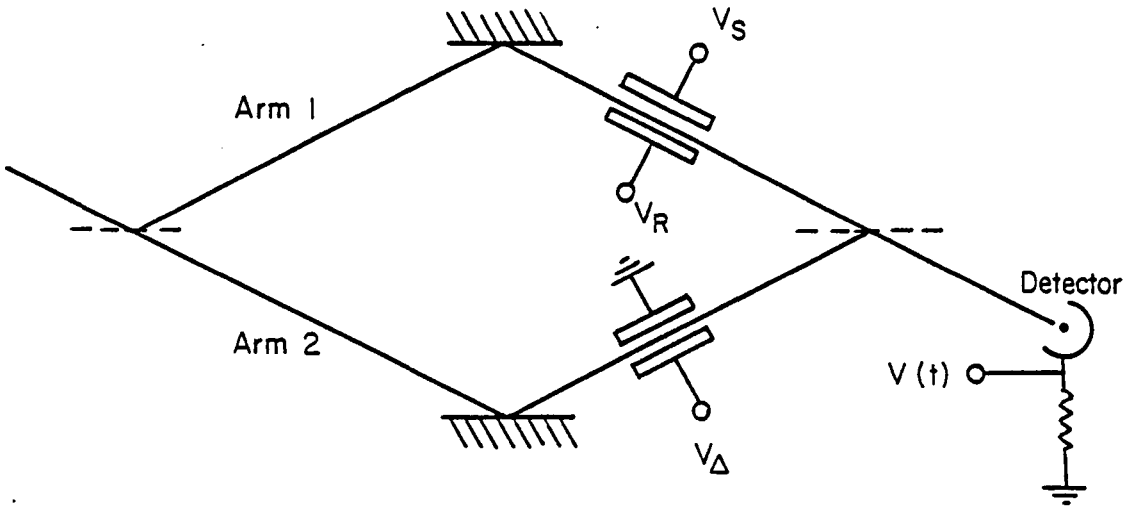

FIGURE III-1. SIMPLE INTEGRATED OPTICAL MACH ZEHNDER INTERFEROMETER IN AN ELECTROOPTIC WAVEGUIDE.

In Eq. III-3, the phase shifts s_i and r_i are assumed to be controllable on a channel-by-channel basis whereas Δ is a uniform phase shift which can be applied across all of the reference channels. Each s_i and r_i is determined by an electric field and is therefore proportional to the difference of two voltages. In the device as it has been considered to date, all meaningful operations are performed on the phases s_i and r_i and not on the amplitudes S_i and R_i. We will assume that a uniform plane wave is coupled into the device so that $S_i = S$ and $R_i = R$, where R and S are constants, for all i. It should be pointed out that an additional degree of computational freedom might be introduced if the values of the $S_{i's}$ and $R_{i's}$ could be varied individually. Since this feature is not built into the present device it will be ignored in this treatment.

It can be seen from Eq. III-3, that the complete dynamic range of the preprocessor can be realized only when R = S. We will, in the rest of this treatment take R=S=A, but before proceeding, we will show that this is a reasonable step and that R=S is a condition which is easily obtained experimentally.

The preprocessor as described thus far is a Mach-Zehnder interferometer with an internal means for controlling the wavefronts. The values of S and R of interest are measured at the detector. If I_o is the input intensity then

$$R^2 = I_o(1-f_1)f_2 \qquad \text{(III-4a)}$$

and

$$S^2 = I_o f_1(1-f_2) \qquad \text{(III-4b)}$$

where $f_1(f_2)$ is the diffraction efficiency of the beam splitter (beam combiner). Equating S and R gives $f_1 = f_2$. Therefore, equality of the signal and reference amplitudes at the detector is achieved by fabricating beam splitters with equal efficiencies.

The voltage V at the detector will be proportional to I. If the proportionality constant is $\eta/2A^2$ we can write

$$V = \eta\frac{I}{2A^2} = \eta \sum_{k=1}^{N} [1 + \cos(\varepsilon_i - \Delta)] \qquad \text{(III-5)}$$

Where $\varepsilon_i = s_i - r_i$ is the phase difference in the i^{th} channel due to the individually induced phase shifts s_i and r_i. In the most general view of the device, the components of four N-dimensional vectors can be introduced, one on each of the four electrode sets. In this case

$$\varepsilon_i = s_i - r_i = \frac{2\, n^3 r}{\lambda} \frac{\ell_s}{d_s} (V_{i\alpha} - V_{i\beta}) - \frac{\ell_r}{d_r} (V_{i\delta} - V_{i\delta}) \qquad \text{(III-6)}$$

Here n is the mode index, r the appropriate electrooptic coefficient, ℓ_i and d_i the length and width of the electrode gaps in the signal and reference arms and the subscripts α, β, γ refer to the four electrical signal ports denoted by V_s, V_r, V_Δ and ground in Fig. III-1.

The present treatment will be restricted to the case where $r \equiv 0$, that is there are no phase perturbations in the optical reference wavefront. Eq. (III-6) may be the basis for further generalization. When $r_i = 0$, Eq. (III-5) reduces to

$$V = \eta \sum_{i=1}^{N} [1 + \cos(s_i - \Delta)] \qquad \text{(III-7)}$$

If we now reinsert the explicit dependence of S_i upon the applied voltages as indicated for the one channel device in Fig. III-1, we get

$$V = \eta \sum_{i=1}^{N} [1 - \cos(RV_{Si} - RV_{Ri} - \Delta)] \qquad \text{(III-8)}$$

where R is a proportionality constant which includes the factors displayed in Eq. (III-6).

Vector Subtraction

Using the standard trigonometric identity for cos(x-y), Eq. III-6 may be rewritten as

$$I = \eta \sum_{i=1}^{N} [1 + \cos R(V_{Si} - V_{Ri}) \cos \Delta - \sin R(V_{Si} - V_{Ri}) \sin \Delta] \qquad \text{(III-9)}$$

If we chose V_Δ such that $\Delta = \pi$ we have

$$I = \eta \sum_{i=1}^{N} [1 - \cos R(V_{Si} - V_{Ri})] \qquad \text{(III-10)}$$

If $R(V_S - V_R) << 1$ for all i we can retain only the first two terms of the Taylor's series expansion and get

$$I = \eta \sum_{i=1}^{N} R^2 (V_{Si} - V_{Ri})^2 = \text{const} \times d_{SR}^2 \qquad \text{(III-11)}$$

where d_{SR} is the scalar distance defined in Eq. 1. Therefore, as long as the difference between the signal and reference sets is small enough to allow the simple approximation to the cosine function, the interferometric device can perform the desired vector subtraction. For larger differences between the two voltage sets there will still be a meaningful output, but the approximation to the true vector difference will be degraded.

Sensitivity

In the notation of Eq. (III-7), the sensitivity of the device may be defined by its response to a small variation in a particular s_j, all other $s_i = 0$. For vanishingly small ∂s_j we find

$$\frac{1}{\eta} \frac{\partial V}{\partial s_j} \Big|_{s_j = 0} = \sin\Delta \qquad \text{(III-12)}$$

so for small signals

$$\frac{1}{\eta} \partial V = \partial s_j \sin\Delta \qquad \text{(III-13)}$$

Eq. (III-13) can be rewritten as a sum over all channels, so the device produces an output which is the product of the magnitude of a vector difference and a scalar sine function. Note that this is a differential output which appears over the D.C. background given by Eq. (III-7) when all $s_k = 0$.

We see that the d.c. level, and therefore the photon noise at the detector, is minimized when $\Delta = \pi$. However, this is also the minimum signal condition. When $\Delta = \pi$, we must rewrite Eq. (III-13) more exactly as

$$\frac{1}{\eta}\,\partial V = \partial s_j \sin(\partial s_j - \Delta) = -\partial s_j \sin \partial s_j = -(\partial s_j)^2 \qquad \text{(III-14)}$$

The minimum noise condition is also the minimum signal condition. The differential signal is maximized when $\Delta = 0$, a condition which also results in maximum d.c. background and maximum photon noise. If the preprocessor is going to be operated in the straightforward vector-subtraction mode, then optimum value for Δ can be determined once the detector noise characteristics, desired response time, and minimum signal level have been specified. If some value of Δ other than π is used, then some electronic method will be required to reject the d.c. background. This could, for example, be accomplished by simple capacitive coupling, by the use of a pulse height discriminator or, most probably, by using a differential amplifier.

IV. PREPROCESSOR DESIGN

DESCRIPTION OF THE IOC

The preprocessor is an integrated optical circuit designed to perform the operation of subtraction of two 16-dimensional vectors. Its final design was the result of an evolutionary process which was influenced by a number of factors including the results of a number of intermediate efforts which were devoted to the fabrication and characterization of most of the individual components. The results of these efforts were evaluated in terms of the interdependent criteria of high performance and ease of fabrication. However, it will probably require several more iterations before the optimum design and fabrication techniques are achieved.

A scale drawing of the device is shown in Figure IV-1. It consists of a number of optical and electrical components most of which are not shown clearly in the Figure because of the extremes of size and aspect ratio of the various components. Enlarged views of these components are presented later in this section.

As shown in Figure IV-1, the light path in the IOC is defined by a titanium-infused waveguide. Light from a He-Ne laser is coupled into the waveguide by a rutile input prism which is clamped on to the broad fanout region of the Ti pattern. The guided beam, which is about 1 mm wide is bifurcated by the grating beam splitter. The two beams progress through the 0.8 mm-wide channels to the horn structures (not resolved in Fig.IV-1) which first segment the beams and then couple the segmented beams into sixteen 7 μm-wide channels. These channel waveguides, which are not indicated explicitly in the figure, curve through an angle of 20° and lead each of the segmented beams between 16 pairs of electrodes which are arranged so that they can impart a phase shift proportional to $(V_{Si} - V_{Ri})$ to each of the 16 segments. The 16 components of each beam are then reassembled by reversed horn structure and the two segmented plane waves are recombined at the beam combiner which is a surface grating identical to the beam splitter. Light from both arms is then coupled out to detectors.

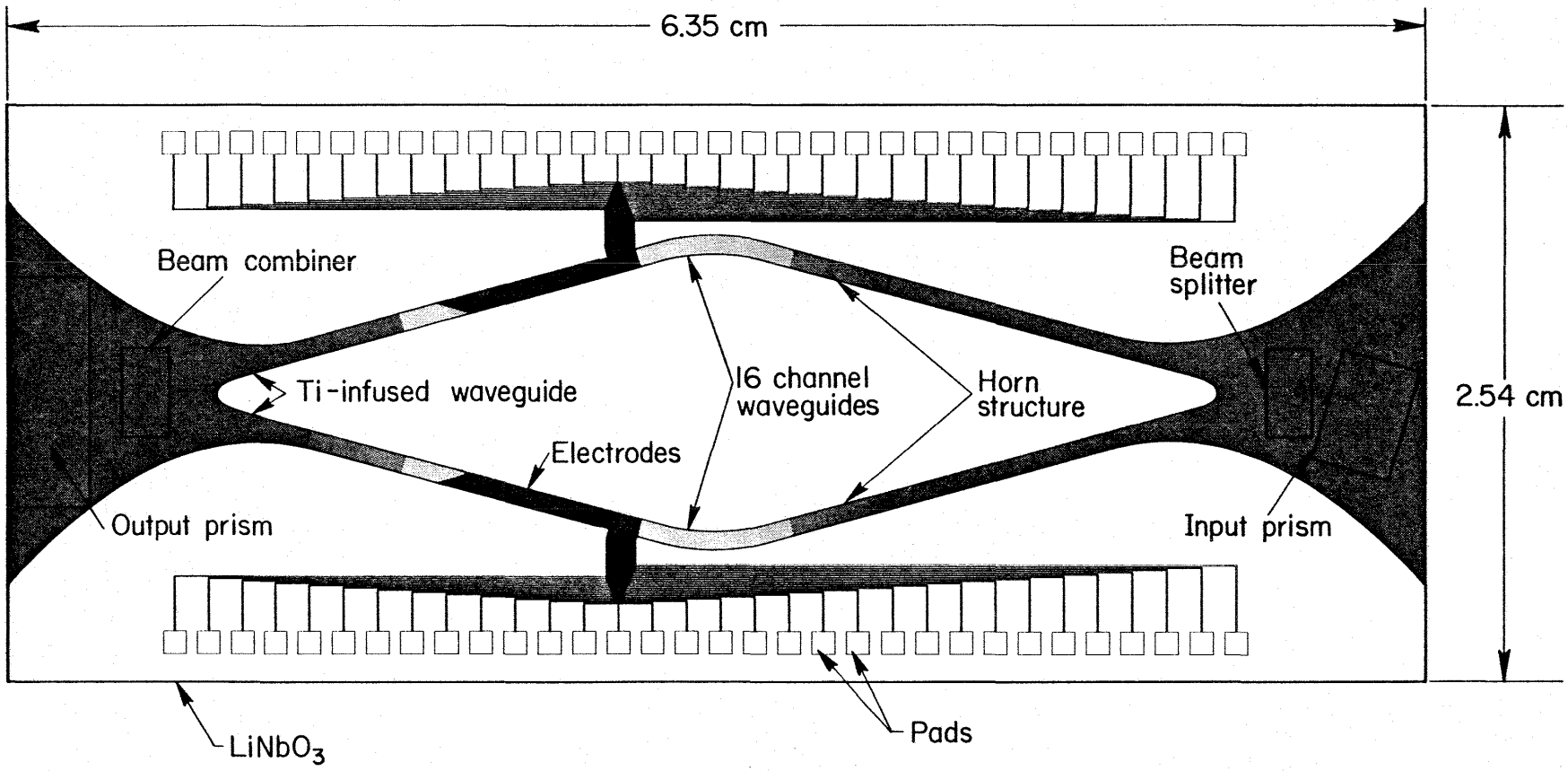

FIGURE IV-1. SCHEMATIC DIAGRAM OF THE PREPROCESSOR LAYOUT. THE Ti-INFUSED WAVEGUIDE REGION IS SHOWN IN OUTLINE. THE SCALE DOES NOT ALLOW INCLUSION OF 7 μm CHANNELS OR ELECTRODE DETAILS.

In operation, the bottom arm, which is the optical reference arm, has its electrodes connected so that the phase shift Δ can be applied uniformly across all 16 channels. The upper, or signal arm has electrodes which can be addressed independently. When all $V_{Ri} = V_{Si}$ for the signal arm, a minimum signal is detected at the appropriate output.

Before discussing the individual components in detail, there are several general features of the processor which should be pointed out. The design is entirely symmetric which has two significant benefits. First, the interferometer should function more perfectly than in an unsymmetric design since the optical paths are identical. Second, since the a and c crystallographic axes of the $LiNbO_3$ are parallel to the long and short edges of the substrate, respectively, the device should respond symmetrically and therefore be relatively insensitive to temperature changes. Another feature of the device is, that in spite of its complexity, there are only three major fabrication steps, the photolithographic definition and infusion of the titanium pattern to form the waveguide, the photolithographic definition of the electrodes and the holographic exposure of the grating structures. These steps are discussed in detail in Section V.

PREPROCESSOR COMPONENTS

Substrate

The laboratory models of the preprocessor are fabricated upon a y-cut slab of $LiNbO_3$ with nominal dimensions of 2.5" x 1" x 0.040". The material used is "selected optical grade" $LiNbO_3$ purchased from Crystal Technology Inc.

Coupling

Input and output coupling is accomplished using rutile prisms. To simplify packaging and to reduce cost, the input prism has a base dimension of 5 mm x 3.5 mm rather than the 10 mm x 7 mm used in previous experiments. The output prism dimensions are 10 mm x 3.5 mm to allow it to pass both output beams. The prisms have been purchased from Adolf Meller Inc.

Waveguides

The entire optical path is a titanium-infused single-mode optical waveguide which is used to guide the TM_0 mode. The titanium is deposited on the $LiNbO_3$ substrate by electron-beam evaporation and the waveguide pattern is defined by photolithographic techniques. The details of the photolithographic mask making and pattern definition are discussed below.

Channels

The processor design requires that, in the data input and in the phase-shifter regions of the beam path, the signal and reference beams be confined to narrow channels. The advantages of channelizing these regions are (1) increased sensitivity, i.e., increased $\Delta\phi/V$; (2) reduced diffraction effects; and (3) improved uniformity of phase shifts. It is necessary to begin the narrow channels before the curved region of the waveguide since curvature losses are inversely proportional to the channel width.[2]

The major criterion for the selection of the channel waveguide parameters is the minimization of optical loss in the device. Our experiments have indicated that the following parameters are optimal.

Channel width	7 μm
Titanium thickness	750 Å
Infusion time	5 hrs
Infusion temperature	1000°C

Under these conditions we anticipated waveguide losses of <2 dB/cm for the straight sections with an additional 10 dB/cm for the curved sections. Since the loss for the 0.8 mm guides is expected to be less than the loss for the 7 μm channels, the overall optical loss should be less than 16 dB. The interchannel crosstalk was expected to be less than 20 dB.

As can be seen in Figure IV-1, the titanium infused pattern extends from one end of the substrate to the other and is symmetric about the long axis of the device. The symmetry is required by the optical considerations, but is also useful in that it considerably reduces the cost and difficulty of mask fabrication. The broad pads at either end of the device couple smoothly

into the 0.8 mm-wide channels. The pads accommodate both the coupling prisms and the grating beam splitters.

The broad pads are joined to the horn region by 0.8 mm-wide channels. The horns function to segment the beam into 16 parallel channels. The layout of the device is such as to provide the maximum straight channel length in the electrode region while minimizing the overall length of the narrow channels. This is done to minimize the required operating voltage and to localize, in so far as is possible, the regions which require high resolution lithography.

Horn Structure

In this section, we discuss the design of the structures (horns) used to separate a beam into sub-beams, constrict them to narrow channels, then expand them and recombine them into a single, broad, beam again. The design developed here is suitable for both Ti-infused and ion-milled channel waveguides.

Burns, et al,[3] have developed a design for parabolic horns that effect an adiabatic (i.e., radiationless) transition between two waveguides of different widths. The pertinent geometry, with notations used, is shown schematically in Fig. IV-2. The design equation is

$$W^2(z) = \frac{2\alpha\lambda_o}{n_b} z + W_o^2 \qquad \text{(IV-1)}$$

where λ_o is the free-space wavelength of the light used, n_b is the bulk index of refraction for $LiNbO_3$, and α is a constant, $\alpha \leq 1$, given by

$$\alpha = \theta_h(z)/\theta_p(z) \quad . \qquad \text{(IV-2)}$$

$\theta_p(z)$ is the mode propagation angle for a waveguide of width z. z is measured from the small end of the horn. Horns designed with $\alpha = 1$ have been found by Burns et al to have low mode conversion losses, i.e., more than 90% of the light passed through the horn without mode conversion (to higher-order lateral modes in the horn region); hence, we take $\alpha = 1$. If W_o and W_{max} are specified, then the length of the horn is given by

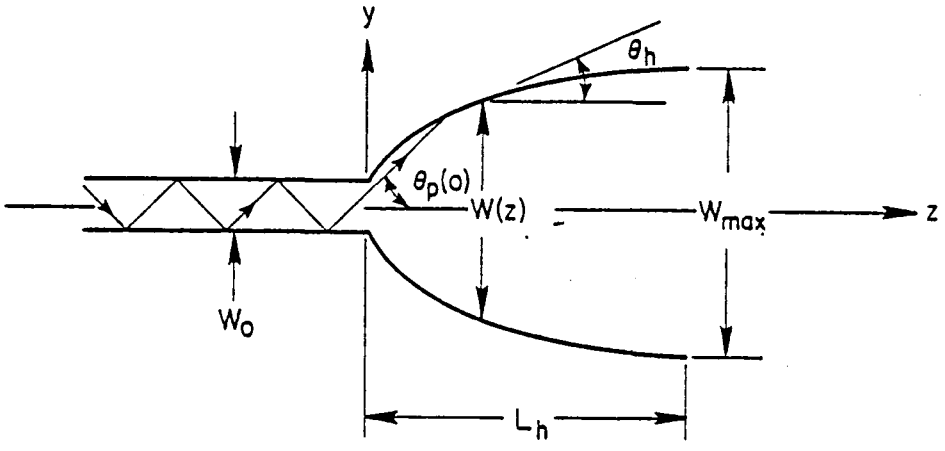

FIGURE IV-2. GEOMETRY AND NOTATION FOR DESIGN OF PARABOLIC HORNS.

$$L_h = (W_{max}^2 - W_o^2)/(2\lambda_o/n_b) \quad . \qquad \text{(IV-3)}$$

Clearly the horn length is dominantly determined by W_{max}. For $LiNbO_3$ ($n_b = 2.200$) and $\lambda_o = 0.633$, the demoninator is

$$\frac{2\lambda_o}{n_b} = 0.575 \quad .$$

For high sensitivity to electrooptic phase shifts, it is desirable to have W_o very small so that the electrode spacing can be minimized. To maintain 10 μm electrode spacing and to allow sufficient clearance between the electrodes we chose 7 μm as a concenient channel width.

The individual horns were designed according to the criteria discussed above. Their dimensions are shown schematically in Figure IV-3. The horns couple smoothly into the 7-wide channels which then curve through a 20 degree arc with an average radius of curvature of 1 cm. After passing through the electrode region, the 16 individual beams are reassembled into a single wide beam by a second set of horn structures.

Wavefront Perturbation

The most important property of the waveguide structure is its ability to reassemble a light beam into a reasonable approximation of the wavefront incident upon the structure. To examine this property, the experimental arrangement shown in Figure IV-4 was employed to test a straight waveguide segment in which horn structures were used to divide a 0.8 mm-wide beam into sixteen 10 μm-wide segments and then recombine these into a single 0.8 mm-wide beam. The waveguide pattern is shown in Figure IV-5. The 1 x mask was fabricated at Qualitron Corp. from Rubylith masters cut at Battelle.

The object of the measurement was to examine the phase perturbation introduced during the segmentation and reassembly of the 0.8 mm-wide beam. Both arms of the interferometer shown in Figure IV-4 contain identical lenses. The reference arm contains a 0.8 mm aperture. The purpose of these components is to ensure that both the signal and reference wavefronts

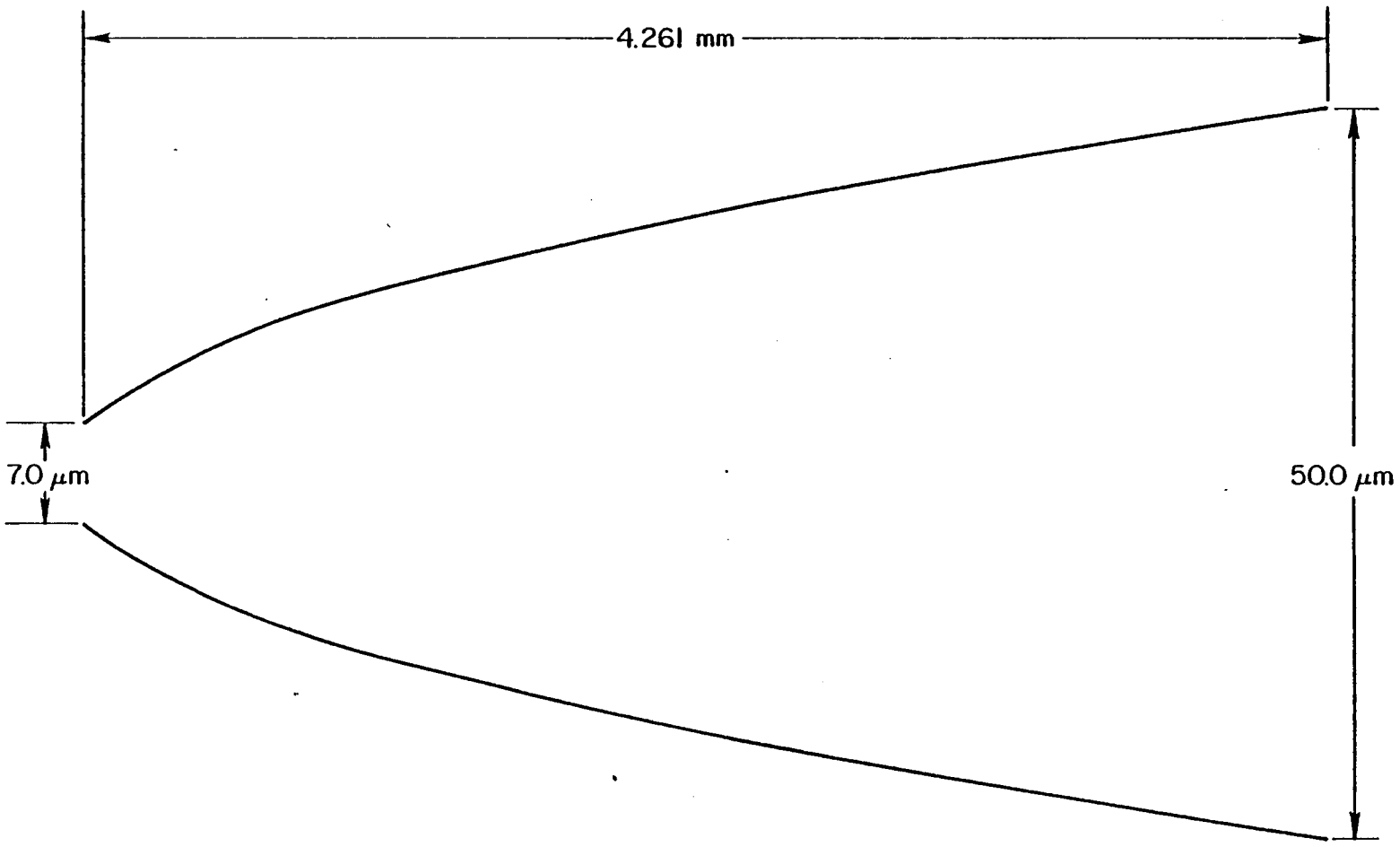

FIGURE IV-3. 7 μm-to-50 μm PARABOLIC HORN. NOTE THE 50-FOLD EXPANSION OF THE VERTICAL AXIS.

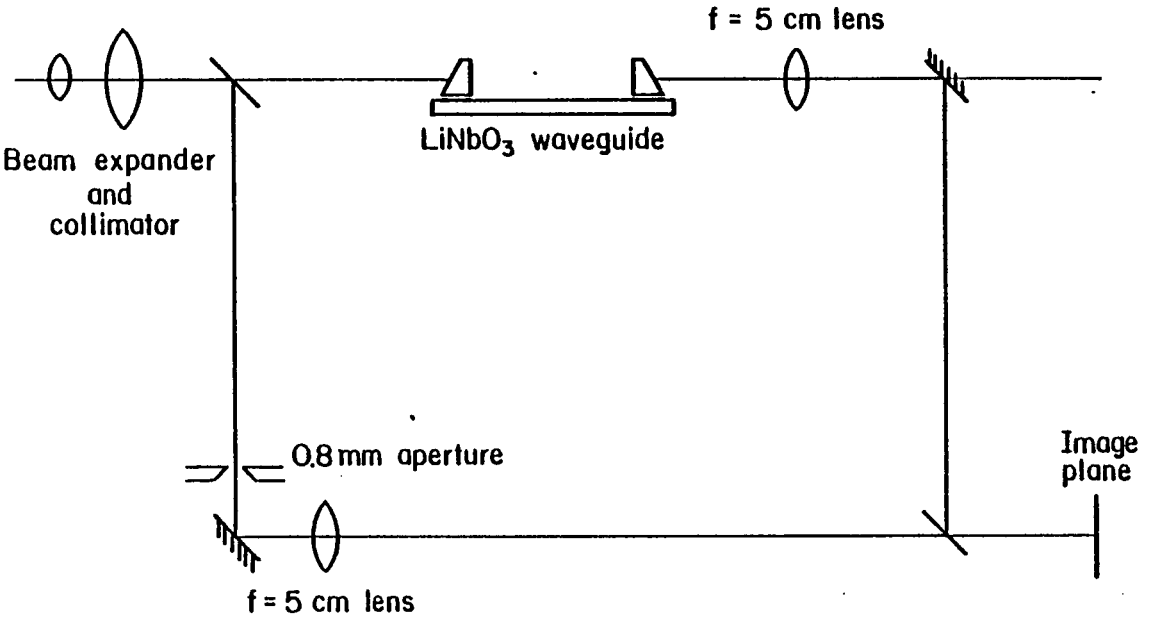

FIGURE IV-4. SCHEMATIC OF LABORATORY APPARATUS FOR EXAMINATION OF WAVE-FRONT PERTURBATION DUE TO CHANNEL WAVEGUIDE STRUCTURE.

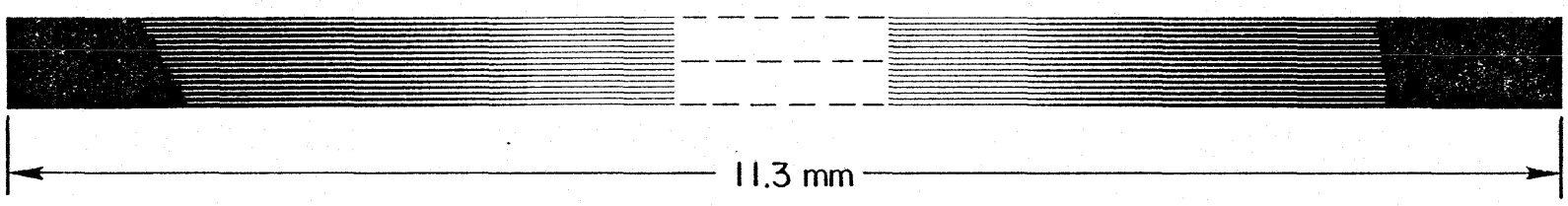

FIGURE IV-5. SIXTEEN 10 μm-WIDE CHANNELS JOINED BY HORNS AT EITHER END (∿ 20X).

exhibit the same curvature, exclusive of any perturbation introduced by the waveguide structure.

Observations using the arrangement depicted in Figure IV-4 were made with the output coupler located on the short 0.8 mm-wide region. The first observation was made by adjusting the position of the lens in the signal arm so that the ends of the 16 individual channels were in focus. Sixteen bright spots were seen in the interference pattern which, by shifting the phase of the reference beam could be simultaneously extinguished. This provided the first indication that the phase of the input beam was preserved as it was segmented and guided through the channels.

The purpose of the next experiment was to examine the process of optical subtraction using the wavefront as reassembled by the horn structure. To do this, the coupling spot was imaged rather than the ends of the horns. The output indicated about a 10% structure across the wavefront, most of which was ascribable to phase rather than amplitude effects. By shifting the phase of the reference beam the overall amplitude could be reduced by about 50% with a similar reduction in the structure. The production of a better null was limited by the fact that the apparatus used was not capable of equilibrating the intensities of the signal and reference beams. However, the uniform reduction of the output intensity acrosss the full width of the signal beam indicated that a much better null would be achieved using a full symmetric interferometer.

Beam Splitter and Beam Combiner

The original plans called for these two elements to be fabricated by exposing a photoresist layer to the periodic pattern formed by the intersection of two coherent .488 μm-beams from an Ar-ion laser. Gratings were first made with a frequency of 1800 lines/mm, giving a 15 degree Bragg angle for the guided 6328 μm He-Ne laser beam. To increase diffraction efficiency the grating frequency and the Bragg angle were reduced to 1200 lines/mm and 10 degrees, respectively to avoid exceeding the resolution limits of the resist.

In the final design the photoresist grating was abandoned entirely in favor of an As_2S_3 grating which is exposed by the same holographic procedure. The As_2S_3 gratings are used because we are able to obtain consistantly higher diffraction efficiencies with them than with the photoresist gratings. Diffraction efficiencies of 50% were typically obtained for 2 mm-thick As_2S_3 gratings. This allowed the use of 1mm-thick gratings which have an angular acceptance range of 0.8 mrad, twice that of the resist gratings. This both reduced the alignment requirement and allowed the beam combiner to accept more light from the output ends of the channels. The use of the As_2S_3 gratings may well have been the key to the successful operation of the preprocessor.

Electrode Design

The use of channel guides in the data entry region of the processor allows the use of simple surface electrodes to impress electrical information on the light beam. The basic form and geometry of the electrodes used is shown in Figure IV-6. Difference information is impressed on light in the waveguide channel passing between the electrodes by simply applying the signal voltage for that channel on one electrode and the reference voltage for that channel on the other electrode. The dimensions used for the preprocessor electrodes are given in Table IV-1.

To achieve a suitable in-line design, without carrying thin lines of metallization over large distances, required that we adopt the unsymmetric design of Figure IV-6 and that we use a conventional fan-out scheme. The scheme adopted is pictured in Figure IV-7, which shows a basic electrode pair in its entirety (no scale) and its relation to neighboring electrodes. Dimensions for the fanout and pad regions are given in Table IV-1.

The large disparity between pattern size and detail dimensions prevents a complete display of the pattern in a single figure. Figure IV-8 shows a section near the middle of the pattern, as generated by the very versatile computer code which was developed as an electrode design tool. The figure shows the electrodes, the leadout bundle, and several of the pads with their complete fanout structure. In order to generate this figure the computer

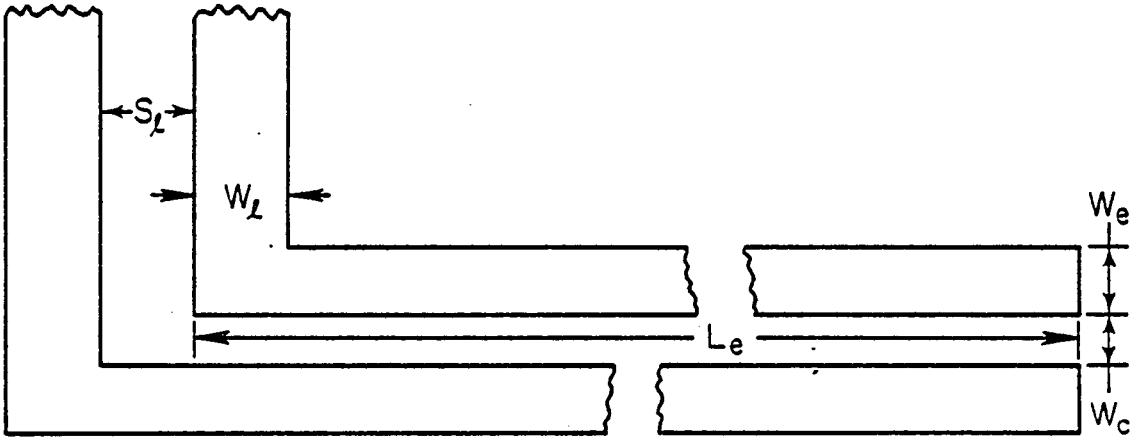

FIGURE IV-6. DETAIL OF ONE ELECTRODE PAIR.

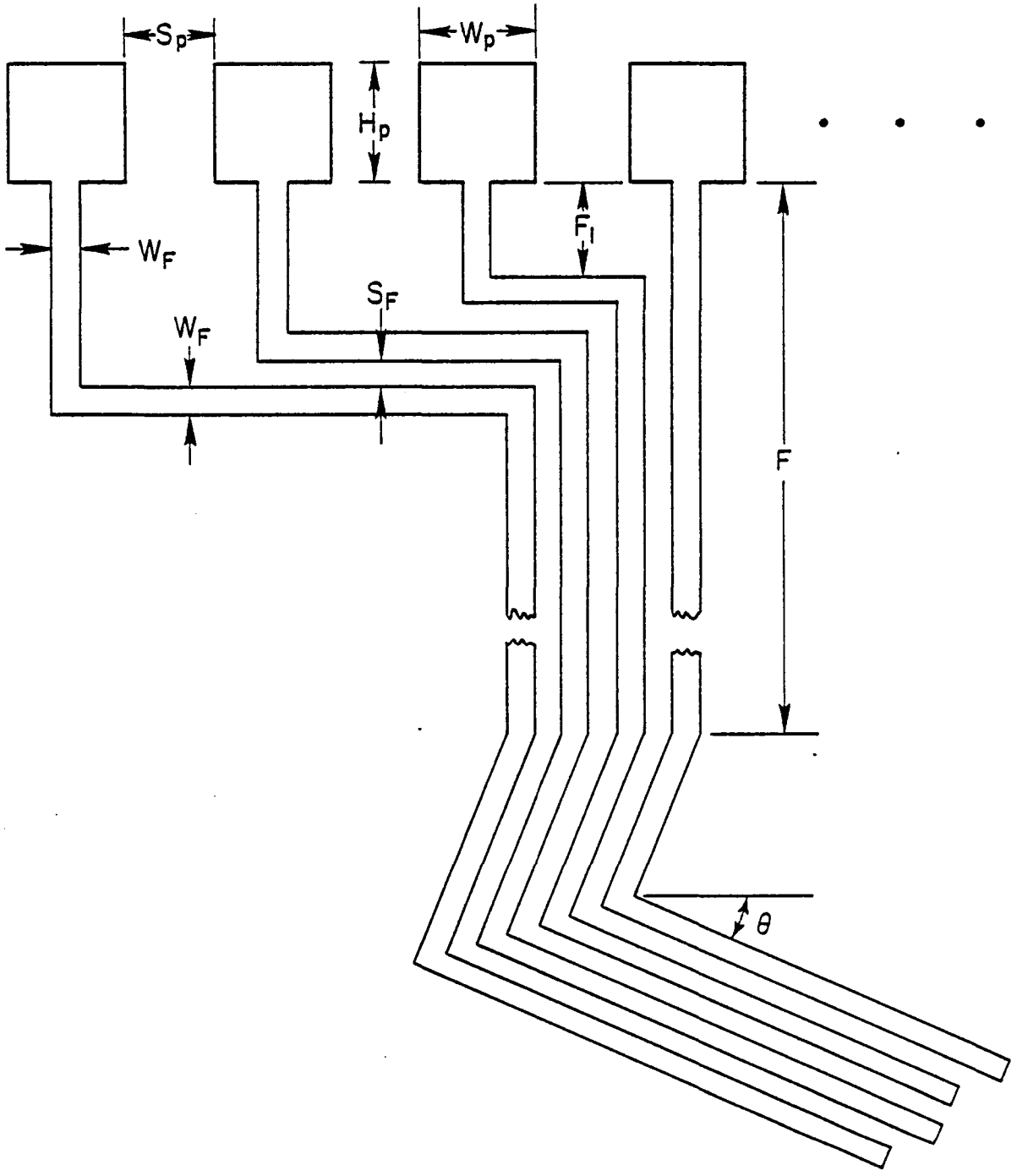

FIGURE IV-7. FANOUT AND PAD DETAIL AND RELATIONSHIP AMONG ELECTRODES (NOT TO SCALE). THE ANGLE θ IS THE INTERFEROMETER HALF-ANGLE.

TABLE IV-1. ELECTRODE PARAMETERS

Item	Meaning	Value
W_e	Width of an electrode	15 μm
S_ℓ	Space between adjacent electrode pairs	10 μm
W_c	Space between electrodes of a pair	10 μm
L_e	Length of an electrode	7.75 mm
W_ℓ	Width of leadout metallization	20 μm
S_ℓ	Space between leadout lines	20 μm
G	Excess leadout length past top electrode edge (before rotation)	100 μm
F	Total fanout height	4.1 mm
F_1	Offset between top horizontal fanout edge and lower pad edge	1.0 mm
W_f	Width of fanout lines	50 μm
S_f	Space between fanout lines	50 μm
Hp	Pad height	1.0 mm
Wp	Pad width	1.0 mm
Sp	Space between pads	0.5 mm
θ	Electrode rotation angle, relative to padline	10°
JC	Number of pad on which leadout bundle is centered	19

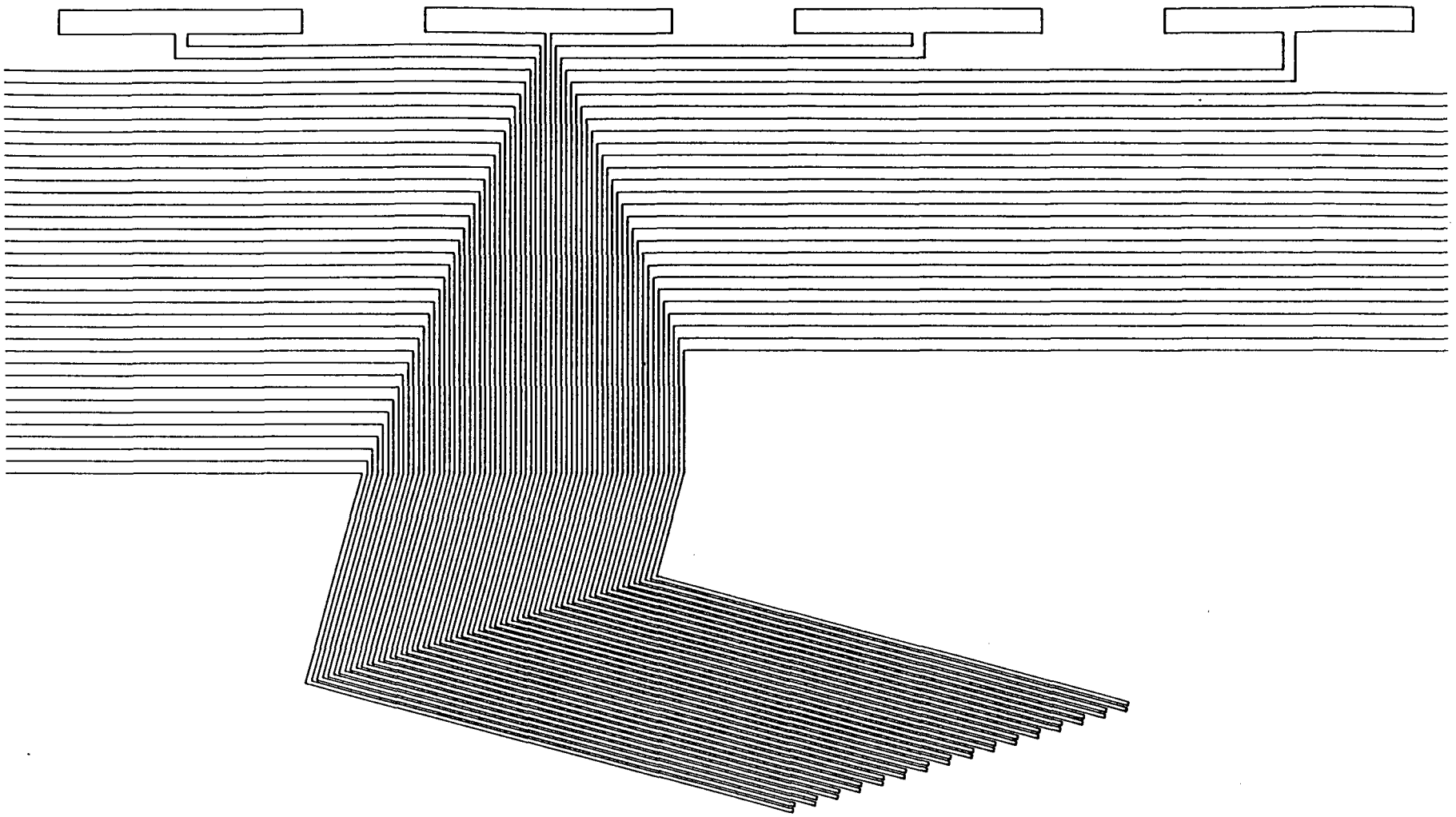

FIGURE IV-8. CENTER OF THE ELECTRODE PATTERN REPRODUCED AT APPROXIMATELY 43 x MAGNIFICATION. THE SQUARE PADS HAVE BEEN TRUNCATED AND THE ELECTRODES SHORTENED FOR THIS FIGURE.

program was altered to produce rectangular pads and shorter electrodes. This allowed reproduction at a sufficiently large magnification to permit resolution of the electrode details.

Source

Although the long term goal of this program was to build a preprocessor which could function using a semiconductor laser, it was felt that it would be more appropriate to use a He-Ne laser for the laboratory demonstration. However, except for the necessity of adjusting the grating spacing of the beam splitter and combiner, the device as constructed is capable of operating at 0.82 μm.

A Coherent Radiation Model 80 He-Ne laser with a nominal output of 2 mw was used in the device characterization.

Detectors

The detector is chosen according to the criteria of sensitivity, noise figure, speed of response, convenience and availability. The overall optical loss of the device was estimated to be about 23 dB. Therefore, 1 mw incident upon the input coupling prism will result in 5 μw at the detector. This is more than enough light for PIN photodiodes such as the Hewlett Packard 5082-series devices. These have response speed in the nanosecond range, sensitivity of 0.5 μA/μw and noise equivalent powers in the range of 3×10^{-14} watts. Output currents will therefore be in the microamp range and the dynamic range will be 80 dB, far greater than that expected from the device itself.

Packaging

Package design has been chosen to satisfy the following goals:

1. Provide protection for the IOC and interconnects.
2. Provide convenient electrical connections.
3. Provide for sturdy mounting of the coupling prisms.
4. Permit safe and convenient transportation.
5. Permit easy access to both input and output optics.

In order to minimize the cost, standard off-the-shelf components were chosen whenever possible. Size minimization was not considered important at this time. Several packages were considered including a dual inline integrated circuit package and one based on the thick film hybrid technology. Cost and availability led to a design that can be fabricated in-house with great flexibility and within a reasonable time frame.

The design focuses around a standard single-sided printed circuit board. The IOC is adhesively attached to a metal substrate and located between the two connection boards (see Figure IV-9). Above that is a metal frame used to clamp prisms on the IOC, the whole structure being ridgidly supported by a thick metal slab attached beneath the circuit board.

The main function of the printed circuit board is to provide electrical interconnect between the IOC and standard ribbon cable connectorrs. 1/16" glass epoxy board with gold plated leads was chosen. An etched pattern with pads for wire bonding forms the interconnect. Leads in this pattern fan out from the two long sides of the IOC to two connectors on opposite sides of the board respectively.

The IOC and circuit board were connected using 0.5 mm copper strips which were attached to the IOC electrical pads by an air dry silver paste. After the bonding is completed, the printed circuit assembly is placed on the metal slab and secured using the upper frame assembly. Prisms are added and clamped in position using fine thread-nylon screws. A box cover can be added for protection during shipment and during testing in the laboratory.

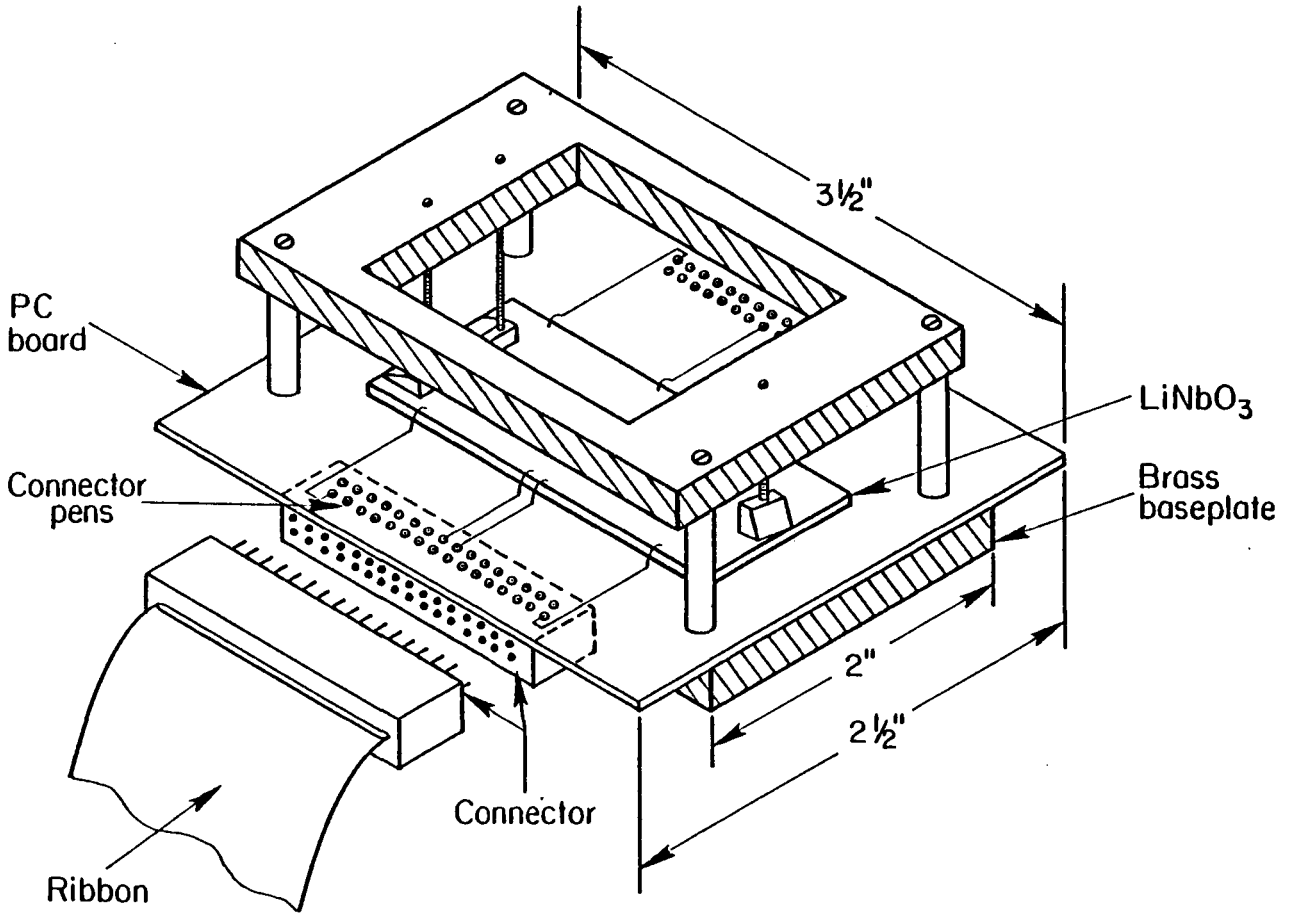

FIGURE IV-9. PREPROCESSOR PACKAGE SHOWING ELECTRICAL CONNECTIONS AND PRISM COUPLERS FOR OPTICAL INPUT AND OUTPUT

V. FABRICATION PROCEDURES

The preprocessor is fabricated in four basic steps:

1. Photolithographic definition an infusion of the titanium waveguide pattern.
2. Photolithographic definition of the electrode pattern.
3. Formation of the beam splitters.
4. Electrical connection and mechanical mounting.

In this section we will discuss those parts of the fabrication procedure which were particularly difficult or for which we had to develop special procedures. We begin with photolithographic mask fabrication, an area which integrated optics technology is pushing close to is current technological limits. We then discuss the entire fabrication process in the sequence in which it is performed.

MASK FABRICATION

Fabrication of the photolithographic masks for the waveguides and/or the associated electrodes presented a particularly challenging problem for the maskmaker because of the large ratio of overall dimension to minimum feature dimension. The problem was solved by sectioning the master patterns, photoreducing each section, then reassembling the sections during the final photoreduction. Some of the joints were sufficiently out of tolerance to produce "knuckles" in the waveguides, an aberration which has proven inconsequential at the present state of development and which can be minimized with further experience with the technique.

Because of the severe tolerance requirement on the electrode structure, two masks were made for the electrode pattern, one for each set. These were then individually aligned using the procedure described below.

The mask fabrication comprised the following steps:

1) Definition of the patterns required, dimensions and path layout; at Battelle.

2) Construction of a computer code to generate set of coordinates for the pattern; at Battelle.

3) From this computer code, generation of a magnetic tape containing instructions for a (flatbed plotter driver) for cutting the pattern in Rubylith; at Battelle.

4) Fabrication of the pattern in Rubylith; this was done by Computer Drafting Company, Haddonfield, New Jersey, on a high-precision, flatbed plotter, using the magnetic tape supplied.

5) Fabrication of chromium-on-glass masks from the Rubylith pattern; this was done by Qualitron Corporation, Danbury, Connecticut, using a two-step photoreduction process with sectioning and reassembling steps as described earlier.

Apart from the aforementioned mismatching of sections at several points, the masks, and therefore the procedures for making them, have proven satisfactory.

FABRICATION OF THE SIXTEEN CHANNEL WAVEGUIDE

Photolithography and Titanium Pattern

The titanium pattern for the 16-channel waveguide was formed by conventional photolithographic techniques comprising a) a metallized substrate, b) positive photoresist (Polychrome PC129SF), and c) wet-chemical etching. Electron-beam evaporation was used to deposit titanium to a predetermined thickness which was monitored by a quartz-crystal thickness monitor. Essential to this process was careful substrate cleaning in mild detergent, thorough water rinsing, and prebake at 300°C before metallization. Microscopic examination of the substrate surface was necessary to assure freedom from particles over the pattern area.

Waveguide Formation

The thickness of the titanium films and the infusion conditions were chosen to minimize the bending losses associated with the curved channels and to provide good coupling efficiency. To minimize the bonding losses required maximizing the index difference between the Ti-infused channel region and the substrate while good prism coupling efficiency necessitated optically

smooth waveguide surfaces. These characteristics were achieved by partially infusing a thick Ti film that was subsequently polished to an optically smooth surface.

Titanium films of .060 μm to .075 μm thickness infused for approximately 12 hrs in an oxygen rich atmosphere at 1000°C produced waveguides with the lowest bending losses. Total losses in the range of 15 dB to 20 dB were typical for these waveguides and in one case the loss was less than 10 dB. Titanium films down to .030 μm thickness were also evaluated, however those waveguides exhibited losses greater than 40 dB. As noted previously the Ti film were not completely infused. Total infusion of the thick Ti films resulted in waveguides with attenuation in excess of 30 dB.

Upon removal from the furnace, the waveguides were characterized by a frosted surface. The rough surface texture resulted in very poor input coupling efficiencies and for this reason the surface required polishing to an optically smooth surface. Syton HT30 on Microcloth with a loading pressure of 20 gr/cm^2 was employed for the polishing procedure. In addition to improving the coupling efficiency, the polishing reduced the scattering losses originating from the rough surface and the Ti compounds present near the surface.

ELECTRODE FABRICATION

Photolithography

Metal electrodes were applied by techniques similar to those used for defining the 16-channel pattern in the titanium layer. In this case, approximately 0.07 μm of aluminum or chromium was vapor-deposited over the substrate with the infused waveguide pattern. Hot-tungsten-boat evaporation was used for the aluminum while chromium was evaporated from a current-carrying tungsten rod having a layer of electroplated chromium.

Registration of the electrode mask by direct observation of the waveguide was simplified by a) the protrusion of the waveguides from the substrate surface as a consequence of indiffusion of a thick layer of titanium, b) enlargement of this protrusion by the polishing operation, and

c) enhancement of the "ridges" by metallization. Visibility was not diminished by the resist layer. Registration marks on the masks were needed only for longitudinal positioning.

Since one electrode mask was used for each set of waveguides, two exposures were required for the complete electrode pattern. This was accomplished simply by masking completely half of the slab during exposure over the other half, then interchanging the electrode and blanking the masks and repeating the process. The continuity and uniformity of the electrodes and associated busses appeared to be unaffected by the surface roughness created by titanium indiffusion and substrate polishing.

SURFACE GRATING BEAM SPLITTERS AND BEAM COMBINER

The surface gratings serve the function of splitting off part of the beam entering one arm of the device and directing it into the opposite arm. At the output end, the surface grating recombines the two beams. To function properly the gratings must be precisely aligned, must diffract at the correct angle and must diffract with a reasonable efficiency.

In the original three channel device the surface gratings were fabricated from a photoresist material. These gratings exhibited relatively low diffraction efficiencies, poor adhesion to the $LiNbO_3$ and a lack of reproducibility. Subsequent experiments have demonstrated that the use of As_2S_3 films as the recording medium overcomes all of these problems. Gratings recorded in this medium typically diffract with efficiencies greater than 20% and exhibit good reproducibility.

Fabrication and Alignment

The surface gratings were fabricated by recording a holographic fringe pattern in the As_2S_3 films deposited on the $LiNbO_3$ waveguide and developing in an appropriate manner. A schematic lay out of the holographic arrangement is shown in Figure IV-10. Included in this set up is the optical system used to align the grating with respect to the 16 channels. The

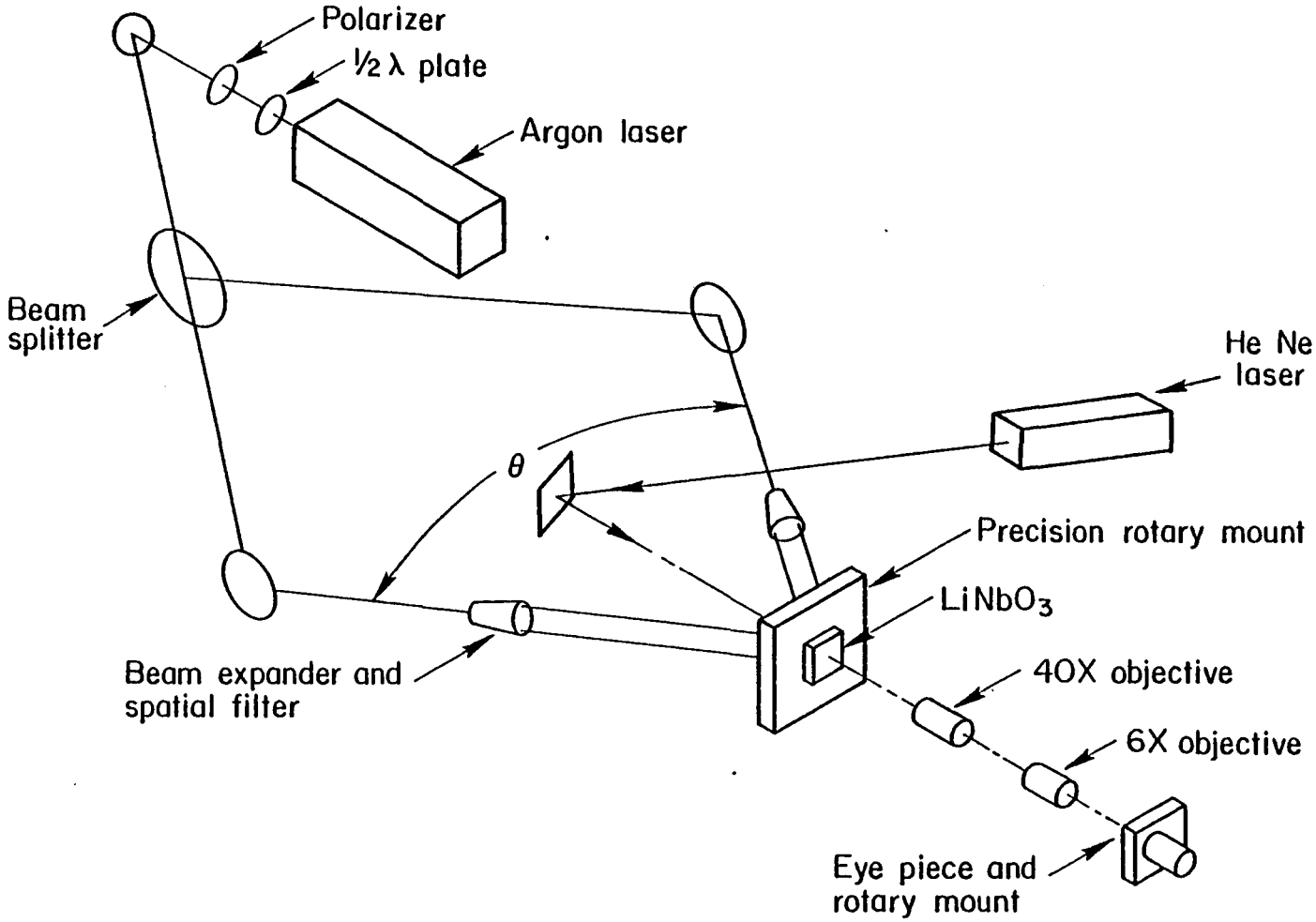

FIGURE IV-10. ARRANGEMENT FOR ORIENTING AND EXPOSING PHOTORESIST BEAM SPLITTER.

angular alignment of the grating and the waveguide channels is a critical step in the fabrication procedure. The acceptance angle of the grating is approximately 0.8 milliradians (grating line pair spacing of 0.830 μm and length of 1 mm), thus the grating and channels must be aligned to an angular accuracy better than ± 0.4 mr. The optical alignment system consist of a microscope that permits observations of the interference generated by the overlapping argon laser beam and the channel pattern infused into the $LiNbO_3$. The eyepiece of the alignment microscope is mounted in a precision rotary mount and contains a cross hair reticle. In the alignment process, one of the reticle cross hairs is aligned with the fringe lines generated by the two overlapping beams. The reticle is then used as a fixed reference mark in which the infused Ti channels are aligned. In the next step the microscope is focused on the surface of the waveguide to observe the 7 μm channels. By using a low power He-Ne laser, to directly illuminate the 7 μm channels, they are easily observed because of interference effects. With the aid of reference reticle, the angle between the two arms of the 16 channel device is measured using the precision rotary mount to which the waveguide is attached. This angle has been measured as 20° 1' 9" ± 15". The waveguide is then aligned so that the bisector of angle between the channels is parallel to the reference reticle. Note that not only must the grating be properly aligned, but the Bragg angle of the grating for the guided beam must not deviate more than ± 0.4 mr from one half of the included angle between the two arms. This angle is controlled by adjusting the fringe spacing of the grating. The technique for evaluationg and measuring that angle is discussed in a later section.

After recording the grating in the As_2S_3, it is then developed by a chemical etching technique and its precise location is defined. The grating, as recorded, occupies an area much larger than needed. To confine the grating to the appropriate region on the waveguide surface, a positive photoresist film is spun over the surface of the waveguide and aligned according to the channel location. The sample is then exposed to a UV source and the exposed resist developed away. Once the resist is removed the developer, undiluted Polychrome D-900, etches away the As_2S_3 film. The remaining resist As_2S_3 film represents the grating beam splitter and beam combiner. The resist coating is removed by washing with methanol and the remaining grating

pattern in the As_2S_3 is developed using Polychrome D900 diluted 20:1 with distilled H_2O. The exposed regions of the grating pattern in the As_2S_3 film are preferentially etched away by the D-900 resist developer to form the surface grating.

Evaluation of Grating Periodicity and Alignment

As noted earlier, the 16 channel device would not function properly if the surface gratings did not diffract at the appropriate angle or were improperly aligned. The precise diffraction angle was determined from measurements of the 16 channel pattern; however, calculating the exact grating spacing was difficult because the effective waveguide index was not known with sufficient accuracy. To compensate for that deficiency, gratings of the approximate spacing were fabricated on a 16 channel waveguide and the resulting angular error in the diffraction was measured. From this measurement the correct grating spacing was determined. The error in the diffraction angle was measured by coupling laser beams in to and out of the waveguide from the two opposite ends. By adjusting these beams to satisfy the Bragg condition for the gratings nearest their input, the angular error in the diffraction angle could be determined by measuring the angular difference between one of the input beams and the output beam from the opposite end of the 16 channel pattern. This same technique was suitable for evaluating the angular misalignment.

VI. PRELIMINARY TESTING OF THE PREPROCESSOR

The initial test of the preprocessor were carried out with the goals of 1) determining that the fabrication procedures did indeed result in a functioning interferometer, and 2) getting a preliminary indication of the device sensitivity. The $LiNbO_3$ slab with completed waveguides, electrodes, and beam splitter, was mechanically and electrically mounted in an arrangement similar to that shown in Figure IV-9. One of the electrodes in each of the 16 electrode pairs in the optical signal arm was grounded. The remaining electrodes were all attached to a common voltage source.

The first step in the test procedure was to observe the output of the interferometer with a low power microscope to see if an intensity change could be observed when a slow voltage pulse was supplied, in parallel, to all sixteen electrodes. In the best possible case one would expect to see a uniform central region in the output beam which varied uniformly in brightness as the voltage changed. The first few devices tested employed 2mm-thick beam splitters. For these we observed only a very small intensity change over a very small region of the output beam. In addition the beam itself was highly structured and the structure was virtually independent of the applied voltage.

The situation described above improved dramatically when the thickness of the grating beam splitters was reduced to 1 mm. The field of view became somewhat more uniform and a significant area changed brightness uniformly as the voltage of the 16 phase shifters was changed in unison. We speculate that this improvement was due to the increased angular acceptance range of the narrower gratings. This reduced the grating alignment criticality and allowed the grating to accept some scattered light which would have been otherwise rejected. This had the result of causing the straight through beam and the diffracted beam to be more nearly equal in intensity, a condition which, as discussed previously, is required for a high contrast ratio. The data shown below was taken by using a multimode optical fiber to couple light from the well behaved part of the output beam to a photomultiplier.

The intial test involved applying 0 voltage pulse to all 16 channels simultaneously on one arm of the device. For this test, the angle of the input beam was adjusted to produce maximum optical output with no voltage applied. During the on time of the voltage pulse, the phase shift introduced into the beam produces destructive interference and a reduction of optical output power. Using pulse amplitudes of -11 volts and a pulse width of 1 m sec an extinction ratio (optical output at 0 Volts/optical output of -11 Volts) of 19 V/0.8 V or 23.7/1 was obtained. An oscilloscope trace of the output obtained is shown in Figure VI-1.

In the next test a -10 V, 100 μ sec-long pulse was applied to only one channel and the optical output observed. The output for a series of such pulses is shown in Fig. VI-2. This optical signal was noted to have an amplitude of approximately 1/16 of that seen when the same pulse was applied to all sixteen channels. This is a good initial indication of uniformity of response across all the channels. With a DC bias voltage of -17 volts applied to the remaining 15 channels and a -10 volt pulse to the single channel, the amplitude of the optical signal deisplayed on the scope was 2.5 Volts. A minimum detectable optical signal with a signal/noise ratio 2:1 was observed with a -5 V pulse and bias voltage of -17 volts. Similar results were observed on other channels. In all cases the phase of the detected optical signal could be reversed during the on time of the voltage pulse relative to the off period could be reversed by varying the DC bias voltage applied to the electrode structures.

At this stage our knowledge of the preprocessor characteristics is still very crude. The device has been shown to respond to pulses as short as 100 microseconds. The device itself should be capable of responding to pulses on the order of 10 nsec, but the limitations of the test electronics used for these initial tests prevented us from verifying this. The overall contrast ratio of about 24:1 for all sixteen channels indicates that the device principle is sound, although the fact that a 5 Volt signal is required to produce a signal-to-noise ratio of 2:1 for a single channel indicates that the

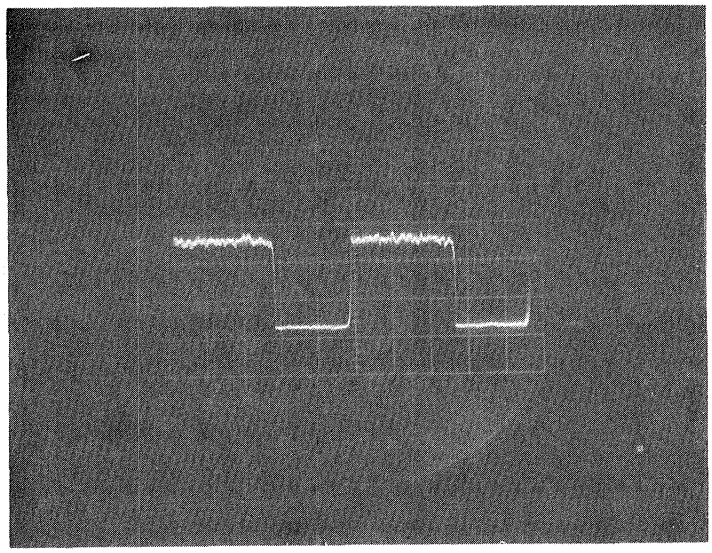

FIGURE VI-1. OSCILLOSCOPE TRACE OF PREPROCESSOR OUTPUT SHOWING RESPONSE TO A -11 VOLT, 1 msec PULSE APPLIED TO ALL 16 CHANNELS. THE EXTINCTION RATIO IS 23.7:1.

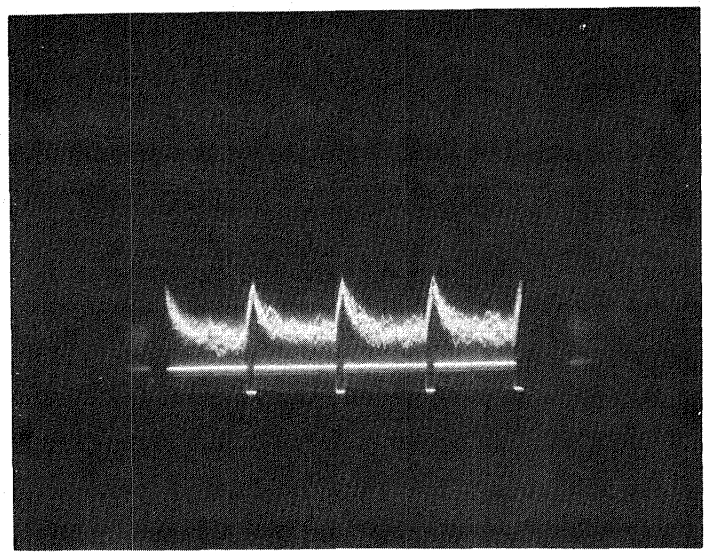

FIGURE VI-2. OSCILLOSCOPE TRACE OF PREPROCESSOR OUTPUT SHOWING RESPONSE TO A -12 VOLT, 100 μ sec REPETITIVE PULSE. THE INPUT PULSE IS SHOWN IN THE LOWER TRACE.

sensitivity is far from optimal. Improved performance is expected to result from a reduction in scatter in the waveguide, and perhaps by further reduction in the beam combiner thickness.

REFERENCES

1. C. M. Verber, D. W. Vahey, R. P. Kenan, V. E. Wood, N. F. Hartman and C. M. Chapman", "An Investigation for the Development of an Integrated Optical Data Preprocessor", NASA-CR-3151, June, 1979.

2. I. A. White, L. D. Hutchinson, and J. J. Burke, "Modal Fields and Curvature Losses in Ti-diffused $LiNbO_3$ Waveguides", Proc. SPIE, 239 (to be published).

3. W. K. Burns, A. F. Milton, and A. B. Lee, "Optical Waveguide Parabolic Coupling Horns", Appl. Phys. Lett., 30, 28-30 (1977).

1. Report No.	2. Government Accession No.	3. Recipient's Catalog No.
NASA-CR-165636		

4. Title and Subtitle	5. Report Date
An Ivestigation for the Development of an Integrated Optical Data Preprocessor	October 1980
	6. Performing Organization Code

7. Author(s)	8. Performing Organization Report No.
C. M. Verber, R. P. Kenan, N. F. Hartman, and C. M. Chapman	
	10. Work Unit No.

9. Performing Organization Name and Address	11. Contract or Grant No.
Battelle Memorial Institute Columbus Laboratories 505 King Avenue Columbus, Ohio 43201	NAS1-14655

12. Sponsoring Agency Name and Address	13. Type of Report and Period Covered
National Aeronautics and Space Administration Washington, DC 20546	Final Report 12/15/78 - 10/30/80
	14. Sponsoring Agency Code

15. Supplementary Notes
Langley Technical Monitor: Marvin E. Beatty III
Final Report

16. Abstract This report discusses the results of a program which culminated in the successful fabrication and the preliminary testing of a laboratory model of a 16-channel integrated-optical data preprocessor. The preprocessor was conceived in response to a need for a device to evaluate the outputs of a set of remote sensors. It does this by accepting the outputs of these sensors, in parallel, as the components of a multidimensional vector descriptive of the data, and comparing this vector to one or more reference vectors which are used to classify the data set. The comparison is performed by taking the difference between the signal and reference vectors. The preprocessor is wholly integrated upon the surface of a $LiNbO_3$ single crystal with the exceptions of the source and the detector. He-Ne laser light is coupled in and out of the waveguide by prism couplers. The integrated optical circuit consists of a titanium-infused waveguide pattern, electrode structures and grating beam-splitters. The waveguide and electrode patterns, by virtue of their complexity, make the vector-subtraction device the most complex integrated optical structure fabricated to date. The fact that this device has performed successfully in its preliminary tests is indicative of the progress being made in integrated-optics technology.

17. Key Words (Suggested by Author(s))		18. Distribution Statement
optical data processing	electrooptic effect	Unclassified - Unlimited
integrated optics	vector subtraction	
$LiNbO_3$		
As_2S_3		
Ti-infused waveguides		

19. Security Classif. (of this report)	20. Security Classif. (of this page)	21. No. of Pages	22. Price*
Unclassified	Unclassified	51	

* For sale by the National Technical Information Service, Springfield, Virginia 22161

NASA Contractor Report 165636

Distribution List
NAS1-14655

	No. of Copies
NASA Langley Research Center Hampton, VA 23665	
Attn: Report and Manuscript Control Office, Mail Stop 180A	1
William M. Moore, Mail Stop 476	1
Dr. Roger A. Breckenridge, Mail Stop 473	1
Rodolfo Segura, Mail Stop 470	20
NASA Ames Research Center Moffett Field, CA 94035 Attn: Library, Mail Stop 202-3	1
NASA Dryden Flight Research Center P. O. Box 273 Edwards, CA 93523 Attn: Library	1
NASA Goddard Space Flight Center Greenbelt, MD 20771 Attn: Library	1
NASA Lyndon B. Johnson Space Center 2101 Webster Seabrook Road Houston, TX 77058 Attn: JM6/Library	1
NASA Marshall Space Flight Center Marshall Space Flight Center, AL 35812 Attn: Library, AS61L	1
Jet Propulsion Laboratory 4800 Oak Grove Drive Pasadena, CA 91103 Attn: Library, Mail Code 111-113	1
NASA Lewis Research Center 21000 Brookpark Road Cleveland, OH 44135 Attn: Library, Mail Stop 60-3	1
NASA John F. Kennedy Space Center Kennedy Space Center, FL 32899 Attn: Library, NWSI-D	1
NASA Scientific and Technical Information Facility 6571 Elkridge Landing Road Linthicum Heights, MD 21090	24 plus original

	No. of Copies
Dr. Carl C. Aleksoff ERIM P. O. Box 8618 Ann Arbor, MI 48103	1
Mr. Thomas J. Bicknell Jet Propulsion Laboratory Building 183, Room #701 4800 Oak Grove Drive Pasadena, CA 91103	1
Prof. Steven K. Case Dept. of Electrical Engineering University of Minnesota Minneapolis, MN 55455	1
Prof. Stuart A. Collins, Jr. Dept. of Electrical Engineering Ohio State University 2015 Neil Avenue Columbus, OH 43210	1
Prof. James M. Florence Dept. of Electrical Engineering University of Texas Austin, TX 78712	1
Prof. Thomas K. Gaylord School of Electrical Engineering Georgia Institute of Technology Atlanta, GA 30332	1
Prof. Nicholas George Director, Institute of Optics University of Rochester Rochester, NY 14627	1
Dr. Mike Giles White Sands Missile Range Attn: STEWS-ID-T White Sands Missile Range, NM 88002	1

	No. of Copies
Dr. Demitri Psaltis Dept. of Electrical Engineering Carnegie-Mellon University Pittsburgh, PA 15213	1
Prof. William T. Rhodes School of Electrical Engineering Georgia Institute of Technology Atlanta, GA 30332	1
Dr. William Sander U. S. Army Research Office P. O. Box 12211 Attn: DRXRO-EL Research Triangle Park, NC 27709	1
Prof. Alexander A. Sawchuk Electrical Engineering Dept. Image Processing Institute University of Southern California Los Angeles, CA 90007	1
Dr. K. Terry Stalker Sandia National Laboratories Division 4426 P. O. Bxo 5800 Albuquerque, NM 87185	1
Dr. William Stoner Science Applications, Inc. 3 Preston Court Bedford, MA 01730	1
Prof. Armand R. Tanguay, Jr. Depts. of Electrical Engineering and Materials Science University of Southern California Los Angeles, CA 90007	1

	No. of Copies
Prof. Joseph W. Goodman Dept. of Electrical Engineering Stanford University Stanford, CA 94305	1
Dr. Bob D. Guenther U. S. Army Research Office P. O. Box 12211 Attn: DRXRO-PH Research Triangle Park, NC 27709	1
Prof. Marion O. Hagler Dept. of Electrical Engineering Texas Tech University Lubbock, TX 79409	1
Mr. Alan Huang Information Systems Laboratory Stanford Electronic Laboratories Stanford, CA	1
Prof. Thomas F. Krile Dept. of Electrical Engineering Texas Tech University Lubbock, TX 79409	1
Dr. B. V. K. Vijaya Kumar Dept. of Electrical Engineering Carnegie-Mellon University Pittsburgh, PA 15213	1
Dr. John N. Lee Harry Diamond Laboratories Branch 13200 2800 Powder Mill Road Adelphi, MD 20783	1
Dr. Wai-Hon Lee Xerox Palo Alto Research Center 3333 Coyote Hill Road Palo Alto, CA 94304	1

	No. of Copies
Dr. Robert D. Leighty U. S. Army Engineer Research Institute Topographic Labs Fort Belvoir, VA 22060	1
Prof. Emmett N. Leith Electrical and Computer Engineering Dept. University of Michigan Ann Arbor, MI 48109	1
Prof. Hau-Kuang Liu Dept. of Electrical Engineering University of Alabama University, AL 35486	1
Dr. Anthony Vander Lugt Harris Corporation P. O. Box 37 Melbourne, FL 32901	1
Prof. Robert J. Marks II Dept. of Electrical Engineering University of Washington Seattle, WA 98195	1
Mr. Michael A. Monahan Naval Ocean Systems Center NOSC Code 811 San Diego, CA 92152	1
Dr. John A. Neff Program Manager AFOSR/NE Bolling AFB, Washington, DC 20332	1
Prof. Thomas G. Newmann Dept. of Mathematics Texas Tech University Lubbock, TX 79409	1
Dr. William M. Portnoy Dept. of Electrical Engineering Texas Tech University Lubbock, TX	1

	No. of Copies
Prof. Chen S. Tsai Dept. of Electrical Engineering Carnegie-Mellon University Pittsburgh, PA 15213	1
Dr. Carl M. Verber Battelle Columbus Laboratories 505 King Avenue Columbus, OH 43201	1
Prof. John F. Walkup Dept. of Electrical Engineering Texas Tech University Lubbock, TX 79409	1
Prof. Cardinal Warde Electrical Engineering and Computer Science Massachusetts Institute of Technology Cambridge, MA 02139	1
Mr. Harper Whitehouse Naval Ocean Systems Center NOSC Code 5303 San Diego, CA 92152	1
Alan Johnston MS 198-336 JPL Pasadena, CA 91103	1
Gordon Chin Code 693 NASA/Goddard Greenbelt, MD 20771	1
Dr. Martin Sokolowski Code RTE-6 NASA Headquarters Washington, DC 20546	3
Mr. Lee Holcomb Code RSI-5 NASA Headquarters Washington, DC 20546	3

End of Document